Environmental Science & Technology

Article

pubs.acs.org/est

Intermediate Volatility Organic Compound Emissions from On-Road Gasoline Vehicles and Small Off-Road Gasoline Engines

Yunliang Zhao,[†,‡] Ngoc T. Nguyen,[†,‡] Albert A. Presto,[†,‡] Christopher J. Hennigan,[†,‡,§] Andrew A. May,[†,‡,∥] and Allen L. Robinson*[,†,‡]

[†]Center for Atmospheric Particle Studies, Carnegie Mellon University, 5000 Forbes Avenue, Pittsburgh, Pennsylvania 15213, United States

[‡]Department of Mechanical Engineering, Carnegie Mellon University, 5000 Forbes Avenue, Pittsburgh, Pennsylvania 15213, United States

Supporting Information

ABSTRACT: Dynamometer experiments were conducted to characterize the intermediate volatility organic compound (IVOC) emissions from a fleet of on-road gasoline vehicles and small off-road gasoline engines. IVOCs were quantified through gas chromatography/mass spectrometry analysis of adsorbent samples collected from a constant volume sampler. The dominant fraction (>80%, on average) of IVOCs could not be resolved on a molecular level. These unspeciated IVOCs were quantified as two chemical classes (unspeciated branched alkanes and cyclic compounds) in 11 retention-time-based bins. IVOC emission factors (mg kg-fuel^{-1}) from on-road vehicles varied widely from vehicle to vehicle, but showed a general trend of lower emissions for newer vehicles that met more stringent emission standards. IVOC emission factors for 2-stroke off-road engines were substantially higher than 4-stroke off-road engines and on-road vehicles. Despite large variations in the magnitude of emissions, the IVOC volatility distribution and chemical characteristics were consistent across all tests and IVOC emissions were strongly correlated with nonmethane hydrocarbons (NMHCs), primary organic aerosol and speciated IVOCs. Although IVOC emissions only correspond to approximately 4% of NMHC emissions from on-road vehicles over the cold-start unified cycle, they are estimated to produce as much or more SOA than single-ring aromatics. Our results clearly demonstrate that IVOCs from gasoline engines are an important class of SOA precursors and provide observational constraints on IVOC emission factors and chemical composition to facilitate their inclusion into atmospheric chemistry models.

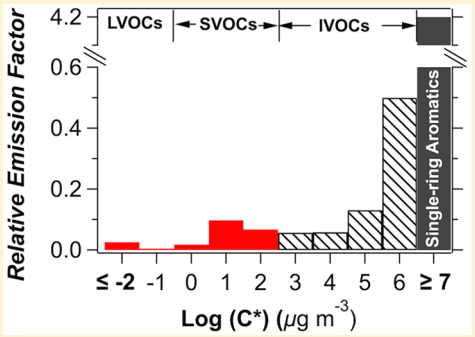

INTRODUCTION

Emissions from on-road light-duty gasoline vehicles (LDGVs) are a major contributor to secondary organic aerosol (SOA) in urban environments.[1−3] Single-ring aromatic compounds (C_6-C_9) are traditionally thought to be the dominant class of SOA precursors emitted from LDGVs.[4−6] However, only a small fraction of SOA formed during photo-oxidation of dilute LDGV exhaust in a smog chamber is explained by single-ring aromatic compounds.[7,8] Gordon et al.[7] hypothesized that the unexplained SOA production was due to emissions of additional SOA precursors, such as intermediate volatility organic compounds (IVOCs), not commonly included in atmospheric chemistry models.

IVOCs are a group of compounds with saturation concentrations roughly corresponding to C_{12}-C_{22} *n*-alkanes.[9,10] Photo-oxidation experiments indicate that individual IVOCs form SOA efficiently.[11−14] The substantial contributions of IVOCs to SOA formation have been suggested by experiments in a traffic tunnel[15] and downwind of a highway[16] and recently substantiated by measurements of IVOCs in the urban atmosphere.[10]

Accounting for IVOCs in SOA models is complicated by the lack of emissions data. A challenge is that IVOC emissions from LDGVs are dominated by unresolved complex mixture (UCM) of coeluted compounds that cannot be speciated when analyzed by traditional gas chromatography/mass spectrometry.[17] Total IVOCs (both speciated IVOCs and IVOC UCM) must be measured to capture the characteristics of IVOC emissions.[9,10,17] Measurements of total IVOCs have been made for LDGVs manufactured prior to 1995,[17] but no quantitative information on volatility and chemical characteristics of the IVOC UCM was reported, which is important for predicting SOA formation.[9,10,13] Furthermore, implementation of new emissions standards has dramatically reduced organic emissions from LDGVs over the past two decades.[18,19] A recent study measured IVOC emissions from on-road vehicles in a traffic tunnel,[15] but it is difficult to isolate the contribution of LDGVs from diesel vehicles in tunnel data.

Received: December 21, 2015
Revised: March 13, 2016
Accepted: March 29, 2016
Published: March 29, 2016

DOI: 10.1021/acs.est.5b06247
Environ. Sci. Technol. 2016, 50, 4554−4563

To investigate their contribution to SOA formation, IVOC emissions have been estimated by scaling nonmethane hydrocarbons (NMHCs), primary organic aerosol (POA), and/or speciated IVOC emissions.[2,4,20,21] However, these estimates are poorly constrained because of the lack of emissions data.[2,4,16] For example, estimates of IVOC emissions based on scaling POA emissions are a factor of 7 lower than those based on scaling naphthalene emissions.[16]

Off-road engines are becoming an increasingly important source of air pollutants in urban environments.[2,3] For example, NMHC emission factors from small off road engines (SOREs) can be 2 orders of magnitude greater than modern LDGVs.[19] We are not aware of any measurements of total IVOC emissions from SOREs.

In this study, IVOC emissions from LDGVs and SOREs were collected during chassis and engine dynamometer testing. Adsorbent samples were comprehensively analyzed to provide quantitative information on the mass, volatility, and chemical composition of IVOCs.[9,10] The relationships between IVOCs and other pollutants were examined to develop methods for estimating IVOC emissions from existing data. SOA production from measured IVOCs was predicted and compared to that from single-ring aromatic compounds and SOA measured in photo-oxidation experiments with dilute exhaust.

MATERIALS AND METHODS

Fleet, Fuel, and Test Cycles. IVOC emissions from LDGVs and SOREs were measured during chassis and engine dynamometer testing at the California Air Resources Board (CARB) Haagen-Smit Laboratory. Detailed information on the test fleet, fuel and test cycles has been reported elsewhere.[19,22] Only a brief description is provided here.

The LDGV test fleet consisted of 42 vehicles recruited from the in-use California fleet. It spanned a wide range of model years (1984−2012), vehicle types, engine technologies and aftertreatment technologies (Supporting Information (SI) Table S1a). For discussion, these vehicles were categorized based on their model years (MY) into "Pre-LEV" (MY prior to 1994), "LEV1" (MY from 1994 to 2003) and "LEV2" (MY in 2004 and later) vehicles. The LEV designation here was only used to refer to a range of model years; it does not necessarily refer to the low-emission vehicle standards. For example, some of the "LEV1" vehicles were certified as Tier 1 (not LEV1) vehicles (SI Table S1a). However, these labels still provide a general indication related to increased stringency of emission standards.[22]

All LDGVs were tested using commercial summertime California gasoline and the cold-start united cycle (UC, SI Figure S1a).[19] A subset of LDGVs (n = 5) was also tested using hot-start cycles to investigate impacts of driving cycles on IVOC emissions (SI Table S1). Three of these vehicles were tested using a hot-start UC (SI Figure S1b); the other two vehicles were tested using both an arterial and a freeway cycle (SI Figure S1c, d).

IVOC emissions were also measured from five SOREs used in lawn and garden equipment, including two 2-stroke and three 4-stroke engines manufactured between 2002 and 2006 (SI Table S1b). These engines met relevant emission standards, but none of them was equipped with any aftertreatment device. The test cycles for these engines depended on engine size and application; the SOREs were tested following CARB procedures for engine certification (SI Table S1b). The same commercial summertime gasoline was used during SORE testing.[19,23]

Emission Characterization. The entire exhaust during each test was diluted inside a constant volume sampler (CVS) using ambient air treated by high-efficient particulate filters. In separate experiments, dynamic blanks were also collected to investigate the potential contribution of background organic vapors to IVOC measurements. Detailed description of the experimental setup and measurement of traditional pollutant data was discussed elsewhere.[7,19,22,23]

IVOCs were collected by sampling dilute exhaust from the CVS through a quartz filter immediately followed by two adsorbent tubes, all connected in series.[9] This sampling train was housed in a heated sampling box (47 ± 5 °C) mimicking the CFR86 protocol. Dynamic blanks (both filters and adsorbent tubes) were collected when the CVS was operated on dilution air (no exhaust) for the same period as a standard driving cycle. Prior to sampling, the quartz filters were prefired at 550 °C in air for at least 12 h and adsorbent tubes were thermally regenerated at 320 °C in the helium flow to reduce their organic background. After sampling, the quartz filters and adsorbent tubes were stored at −18 °C until analysis.

Quantification of IVOCs. The adsorbent samples were analyzed by gas chromatography/mass spectrometry (Agilent 6890 GC/5975 MS) using a capillary GC column (Agilent HP-5MS, 30 m × 0.25 mm) and a thermal desorption and injection system (Gerstel, Baltimore, MD) (SI).[9,10]

Figure 1a shows chromatograms of a typical adsorbent sample. Straight chain alkanes (n-alkanes) and polycyclic aromatic compounds (PAHs) dominate the mass of speciated IVOCs, but they only account for a small fraction of the total IVOC mass (Figure 1a, b). Therefore, quantification of total IVOCs cannot be achieved through speciation analysis.

The mass of total IVOCs (speciated + UCM) was determined using the approach of Zhao et al.[9,10] (SI). Briefly, the total ion chromatogram of each adsorbent sample was separated into 11 roughly equal width retention time bins. Each of these bins centered on the retention time of an n-alkane (C_{12}-C_{22}) and was referred to as the B_n IVOC bin where "n" was the carbon number of the n-alkane in that bin (Figure 1a). The total IVOC mass in each bin was determined using the integrated total ion current for that bin and the total ion current response factor for the n-alkane in that bin (Figure 1b). The uncertainty of using n-alkanes as surrogate standards for the total IVOC mass was estimated to be less than 17% for alkanes and 31% for PAHs based on the analysis of a suite of standard compounds (SI). Following quantification of the total IVOCs, the mass of IVOC UCM was determined by the difference (total IVOC mass minus speciated IVOCs). The IVOC UCM was further classified into unspeciated branched alkanes (b-alkanes) and unspeciated cyclic compounds in each of 11 bins using information from the mass spectrum (Figure 1b, SI).[9,10]

The quartz filter samples were analyzed by GC/MS using the same method, except that the thermal desorption temperature used for the filter analysis was 300 °C instead of 275 °C for adsorbent samples. The quartz filter samples were also analyzed by a Sunset Laboratory EC/OC Carbon Aerosol Analyzer model 3.[9] The OC mass from the EC/OC analysis was converted to OA by multiplying a factor of 1.2.[24,25]

Volatility distributions of IVOCs, semivolatile organic compounds (SVOCs) and low-volatility organic compounds (LVOCs) were derived from the GC/MS data using the n-

DOI: 10.1021/acs.est.5b06247
Environ. Sci. Technol. 2016, 50, 4554−4563

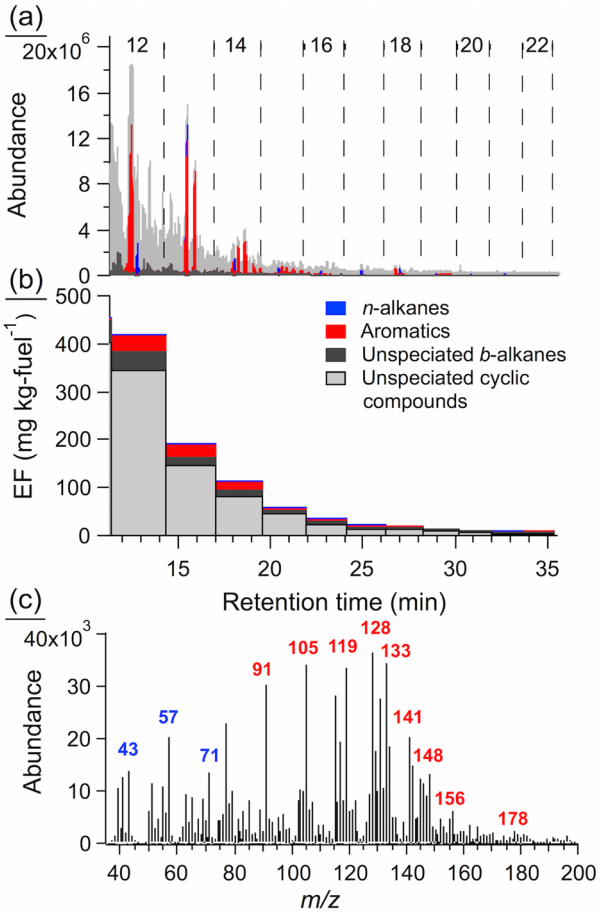

Figure 1. (a) Chromatograms from GC/MS analysis of an adsorbent tube sample collected during a typical light duty gasoline vehicle cold-start UC test. The vertical dashed lines mark the width of each retention-time bin. The number indicates the carbon number of the *n*-alkane in that bin. (b) IVOC EFs in each retention-time based bin for the sample shown in panel (a). (c) Average mass spectrum of the chromatogram shown in panel (a). The mass fragments labeled in blue and red in panel (c) are associated with aliphatic and aromatic compounds, respectively.

alkane in each bin as the surrogate for the saturation concentration of all organics in that bin.[9,10]

Emission Factors. Fuel-based emission factors (EF, mg/kg-fuel) of IVOCs were calculated using the carbon-mass-balance approach. The total fuel carbon in the tailpipe emissions was calculated by summing the carbon in the background-corrected CO_2, CO and NMHC concentrations measured in the CVS reported in May et al.[19]

The IVOC concentrations measured in the dilute exhaust were not corrected for dynamic blanks. The dynamic blank corresponds to an IVOC EF of 5.3 ± 1.1 mg/kg-fuel, based on the average fuel consumption across all UC tests. This corresponds to less than 3%, on average, of the IVOC EF for Pre-LEV vehicles and off-road engines, and less than 18% and 23% of the IVOC EF for LEV1 and LEV2 vehicles. A challenge is that these blanks likely represent the upper limit of contributions of background IVOCs because operating the CVS on clean air promotes evaporation of organics lost to the sampling system walls.[19]

RESULTS

IVOC Emission Factors. Figure 2a compiles the total IVOC EFs for LDGVs tested over the cold-start UC. Although

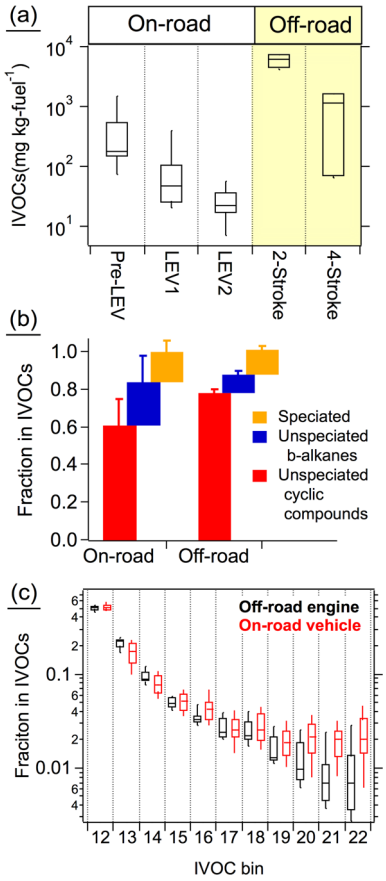

Figure 2. (a) Box-whisker plot of total (speciated + UCM) IVOC EFs for on-road light duty gasoline vehicles operated over the cold-start UC and small off-road engines (SOREs); and (b) mean chemical composition of IVOCs; and (c) box-whisker plot of mass fraction of IVOCs in each retention-time bin. In (a) and (c), the boxes represent the 75th and 25th percentiles with the centerline being the median. The whiskers are the 90th and 10th percentiles. The error bars in (b) are one standard deviation of the mean.

there is a substantial vehicle-to-vehicle variation, newer vehicles that meet more stringent emission standards have, on average, lower IVOC emissions than older vehicles. For example, the median IVOC EF for LEV1 and LEV2 vehicles is 72% and 87% lower than the median Pre-LEV vehicle, respectively. These changes mirror the reduction in NMHC emissions in this fleet.[19]

Five vehicles were tested on both hot- and cold-start cycle. As expected, hot-start cycles have lower NMHC emissions than cold-start tests (SI Figure S2a). However, this was not always observed for IVOCs (SI Figure S2b). For example, the average ratio of hot-start-to-cold-start IVOC emissions is 1.2 ± 0.2 (average ± one standard deviation) versus 0.27 ± 0.18 for NMHC emissions for the three LDGVs tested over both hot- and cold-start UC. The disproportionate change in IVOC versus NMHC EFs between hot- and cold-start cycles is unexpected. It is not an artifact of background contamination. The hot-start IVOC EF is at least a factor of 3 greater than the average dynamic blank, except for one arterial test (SI Figure S2b). Instead, it may indicate that catalytic converters have

DOI: 10.1021/acs.est.5b06247
Environ. Sci. Technol. 2016, 50, 4554−4563

different removal efficiencies for NMHCs and IVOCs.[17] The number of paired hot- and cold-start tests in this test program is relatively small; therefore, more research is needed on the effects of test cycles on IVOC emissions.

Figure 2a also compares the total IVOC EFs for SOREs and LDGVs. The highest IVOC EFs were measured during 2-stroke SORE tests. IVOC EFs for 4-stroke engines vary widely, overlapping with the emissions from Pre-LEV and LEV1 vehicles. The median IVOC EF from 2-stroke and 4-stroke SOREs is 271 and 51 times greater than the median for LEV2 vehicles, respectively. This difference means that SOREs are likely an important source of IVOCs, even though SOREs, such as lawn and garden equipment, only use about 2% of the gasoline consumed by LDGVs.[26] For example, if on-road fleet consisted entirely of LEV2 vehicles, then our data indicates that SOREs would contribute over 50% of total IVOCs from on-road and off-road gasoline engines.

Chemical Composition of IVOCs. Figures 2b and SI Figure S3 compare the chemical composition of IVOC emissions from LDGVs and SOREs (data are in SI Table S2). Speciated IVOCs include *n*-alkanes, *b*-alkanes, *n*-alkylcyclohexanes, *n*-alkylbenzenes, and unsubstituted and substituted PAHs (SI Table S3). In total these species contribute, on average, less than 20% of the total (speciated + unspeciated) IVOC emissions. Naphthalene and substituted naphthalenes (C_{11}-C_{14}) dominate the emissions of speciated IVOCs.

Unspeciated IVOCs (UCM) account for 83% to 89%, on average, of the total IVOC emissions from each class of engines (SI Figure S3a). IVOC UCM was classified into unspeciated *b*-alkanes and unspeciated cyclic compounds in each of 11 retention time bins (Figure 1a, SI Table S3). Unspeciated cyclic compounds are the dominant class of IVOCs, contributing between 59% (LEV2) and 79% (2-stroke SORE) of the total IVOC emissions (SI Figure S3a). For LDGVs, the fractions of unspeciated *b*-alkanes and unspeciated cyclic compounds are consistent between hot- and cold-start cycles.

Figure 2c shows the distributions of IVOCs in the 11 retention-time bins. The distributions are heavily skewed toward more volatile IVOCs, with about half of the emissions in the B_{12} bin. The LDGV IVOC distributions do not depend on test cycle (cold versus hot start cycles). There are some differences in IVOC emissions in the lower volatility bins (B_{20}–B_{22}). For example, the median fraction of IVOCs in the lower volatility bins follows the order of LEV2 > LEV1 > Pre-LEV vehicles (SI Figure S4). Although the mass fraction of IVOCs in these lower volatility bins is small (less than 10%, on average), their contribution to SOA production could be important.

Additional information on IVOC composition can be extracted from the average mass spectra of IVOCs. Figure 1c presents the average mass spectrum of the IVOCs collected during one LDGV test. The most abundant mass fragments have an m/z greater than 90. These mass fragments are associated with aromatic compounds; for examples, m/z 91, 105, and 119 are major fragments of alkylbenezenes.[27] These aromatic mass fragments are more abundant than those produced by electron ionization of aliphatic compounds: C_nH_{2n+1} and C_nH_{2n-1} (for example, m/z 57 and 55).[28] Therefore, aromatic compounds are likely an important component of LDGV IVOC emissions. SI Figure S5 illustrates that IVOC emissions from all LDGVs have similar mass spectral signatures.

IVOC composition also varies with volatility. SI Figure S6 presents the average mass spectra of IVOCs in two volatility ranges, B_{12}–B_{16} and B_{17}–B_{22}. The mass spectra indicate that aromatic compounds are primarily present in the higher volatility (B_{12}–B_{16}) bins while mass fragments of aliphatic compounds are more abundant in the B_{17}–B_{22} bins. Therefore, unspeciated cyclic IVOCs in the lower volatility bins (B_{17}–B_{22}) are predominantly cyclic alkanes versus aromatic compounds in the higher volatility bins (B_{12}–B_{16}).

Estimating Total-IVOC Emissions Using Other Emission Data. Previous studies have estimated total IVOC emissions for SOA modeling by scaling traditional emission data, including POA, NMHCs, and speciated organics.[2,4,21] The quality of these estimates is uncertain due to the lack of direct measurements of total IVOC emissions. The comprehensive measurements performed here allow for a quantitative evaluation of the relationships between IVOCs and other pollutants. In this section we discuss scaling factors for IVOCs using NMHC and POA data. Correlations with speciated IVOCs are discussed in the SI.

Relationship between Total IVOCs and NMHCs. IVOC and NMHC EFs are strongly correlated. For LDGVs operated over the cold-start UC, a linear regression yields a slope (average IVOC-to-NMHC ratio) of 0.04 ± 0.02 and an R^2 of 0.92 (Figure 3a). A similarly strong correlation exists for SOREs (R^2 = 0.94) with the average IVOC-to-NMHC ratio of 0.03 ± 0.02.

The IVOC-to-NMHC ratio in LDGV emissions depends on driving cycle. LDGV IVOC-to-NMHC ratios over the hot-start cycles are greater than those over the cold-start UC; for

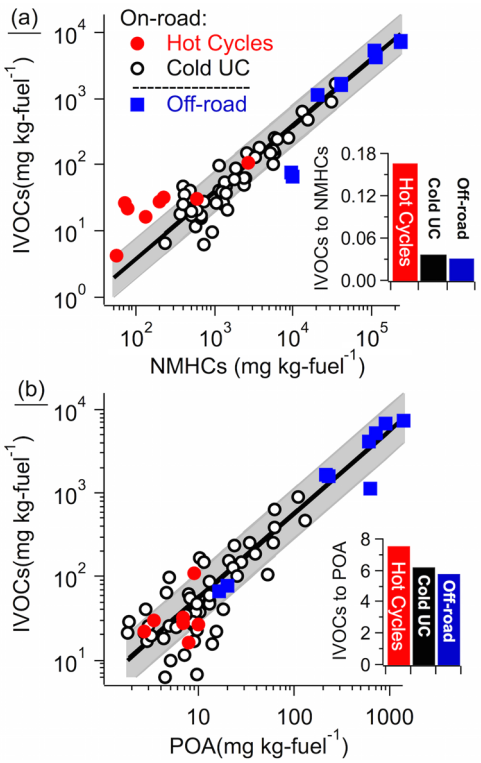

Figure 3. Correlation of total (speciated + UCM) IVOC EFs to (a) NMHC and (b) POA EFs measured during all on-road vehicles and off-road engine tests. The insets in (a) and (b) present the average IVOC-to-NMHC and IVOC-to-POA ratio for each source group. The shaded area in (a) and (b) is the range of 0.5–2 times the slope (the solid line).

DOI: 10.1021/acs.est.5b06247
Environ. Sci. Technol. 2016, 50, 4554–4563

example, the average IVOC-to-NMHC ratio across all hot-start tests is 0.17 ± 0.12 versus 0.04 ± 0.02 for cold-start tests. Further studies are needed to investigate IVOC emissions during hot-start cycles given the limited number of tests performed here. However, our data suggest that the total IVOC emissions from LDGVs would be underestimated if they are based solely on IVOC-to-NMHC ratios measured during cold-start tests.

Although IVOCs are a small fraction of NMHCs, an open question is whether these IVOCs are included in the existing NMHC EFs or if they are lost in the NMHC sampling system.[8,9] If they are lost, IVOC emissions need to be added to the existing NMHC emissions data. Research is needed to determine the contribution of IVOCs to existing NMHC emissions.

The IVOC-to-NMHC ratios measured here are different from the scaling factors developed by previous studies. For example, Gentner et al.[4] proposed an LDGV IVOC-to-NMHC ratio of ~0.01 based on the chemical composition of gasoline fuels.[4] A higher ratio of ~0.02 was measured for LDGVs manufactured prior to 1995.[17] These ratios are smaller than those measured here and therefore underpredict the contribution of LDGVs to atmospheric SOA. However, IVOCs are overpredicted if one assumes that all unspeciated NMHCs are IVOCs, which corresponds to an IVOC-to-NMHC ratio of 0.25.[2,19]

Relationship between Total IVOCs and POA. IVOCs and POA emissions are correlated (R^2 = 0.76) (Figure 3b) with an IVOC-to-POA ratio of 6.2 ± 4.4 for LDGVs over the cold-start UC and 5.8 ± 2.1 for SOREs. There is little variation in the IVOC-to-POA ratios of Pre-LEV, LEV1, and LEV2 vehicles. POA in these ratios is based on bare quartz filter samples collected from the CVS, which is the basis for most POA emission inventories. However, POA measured in this manner (quartz filters collected from CVS) is not representative of atmospheric POA due to the combination of sampling artifacts and partitioning biases.[22] We have not corrected the IVOC-to-POA ratios reported here for those biases because the ratios are intended for scaling existing emissions inventories.

The IVOC-to-POA ratios for LDGVs operated over hot- and cold-start UC are similar (Figure 3b). For the subset of vehicles tested over multiple test cycles, the average IVOC-to-POA ratio is 7.3 ± 4.9 for the cold-start UC versus 8.5 ± 3.9 for the hot-start UC. There are larger differences between the ratios measured during arterial and freeway cycles (average ratio of 3.0 ± 0.9) compared to the cold-start UC data but the number of arterial and freeway experiments was small.

Previous studies have used an IVOC-to-POA ratio of 1.5 to estimate IVOC emissions from both on-road gasoline and diesel vehicles.[20,29] This ratio is based on emissions from a small number of medium duty diesel vehicles.[29] This ratio underpredicts the IVOC emissions from the modern LDGVs tested here by about a factor of 4. An IVOC-to-POA ratio of 1.5 also underpredicts IVOC emissions from modern on-road diesel vehicles.[9]

Schauer et al.[17] measured organic emissions from LDGVs manufactured prior to 1995 operated over the cold-start UC; these data yield an IVOC-to-POA ratio of 2.9, smaller than our measurements for Pre-LEV vehicles. The difference may be due to differences in sampling conditions between the two studies. Schauer et al.[17] collected filter samples at ~25 °C versus ~47 °C in our study. Lower sampling temperature favors collection of SVOCs by quartz filters. The difference in IVOC-to-POA ratios may also be due to actual differences in emissions; given that the pre-LEV vehicles tested here are much older and higher mileage than the vehicles tested by Schauer et al.[17] Given the issues of filter sampling artifacts and partitioning biases, we recommend estimating IVOC emissions by scaling NMHC not POA emissions.

Volatility Distribution of Organics ($C^* \leq 3 \times 10^6$ μg/m^3). The sampling strategy employed here, a quartz filter followed by two adsorbent tubes, captures all organics with an effective saturation concentration (C^*) ≤ 3×10^6 μg/m^3 corresponding to the B_{12} bin.[9] The GC/MS data from these media can be combined to derive the volatility distribution of measured organics, which are classified into three groups based on volatility: IVOCs (C^* = 300−3×10^6 μg m^{-3}, Table S4); SVOCs (C^* = 0.3−300 μg m^{-3}); and LVOCs (C^* < 0.3 μg m^{-3}) (Figure 4).

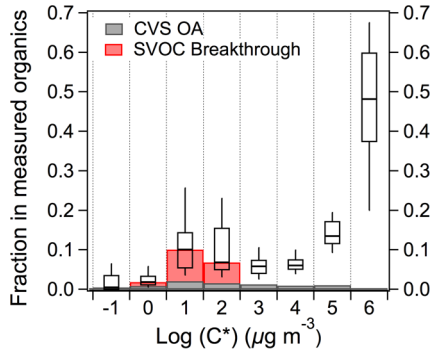

Figure 4. Volatility distribution of organics thermally desorbed by GC/MS analysis of quartz filters and adsorbent tubes collected during the tests for on-road gasoline vehicles operated over the cold-start UC. The distribution is expressed as the mass fraction of the total organics in the 10^{-1} to 10^6 μg m^{-3} bins. The boxes represent the 75th and 25th percentiles with the centerline being the median. The whiskers are the 90th and 10th percentiles. The red-shaded area is the median mass fraction of SVOCs collected by adsorbent tubes downstream of the quartz filter. The gray-shaded area indicates the median mass fraction of organics collected by quartz filters.

Figure 4 presents the volatility distribution of organic emissions from LDGVs (SI Table S5).[9,29,30] IVOCs are the dominant component of the low volatility organic emissions with an average contribution of 77 ± 14%, followed by 21 ± 13% from SVOCs and ~2% from LVOCs.

Sampling Artifacts. It is well recognized that quartz filters are prone to sampling artifacts.[22] Organic vapors adsorbed onto filters are positive sampling artifacts. Evaporation of organic particulate matter creates a negative sampling artifact. The combination of GC/MS analysis and collection of adsorbent tubes allows investigation of these artifacts.

The GC/MS analysis reveals that a small fraction (less than 10% on average) of IVOCs was collected by quartz filters (Figure 4). Under the sampling conditions of these experiments, all of the IVOCs exist as vapors; therefore the IVOCs collected on quartz filters are adsorbed vapors (a positive sampling artifact from the perspective of measuring particulate organic carbon).[22] IVOCs contribute 47%, on average, of total organics collected by the quartz filter. SVOC vapors likely contribute additional positive artifact. Positive sampling artifacts can be corrected for using the organics collected by a quartz filter behind a Teflon filter.[22,31]

DOI: 10.1021/acs.est.5b06247
Environ. Sci. Technol. 2016, 50, 4554−4563

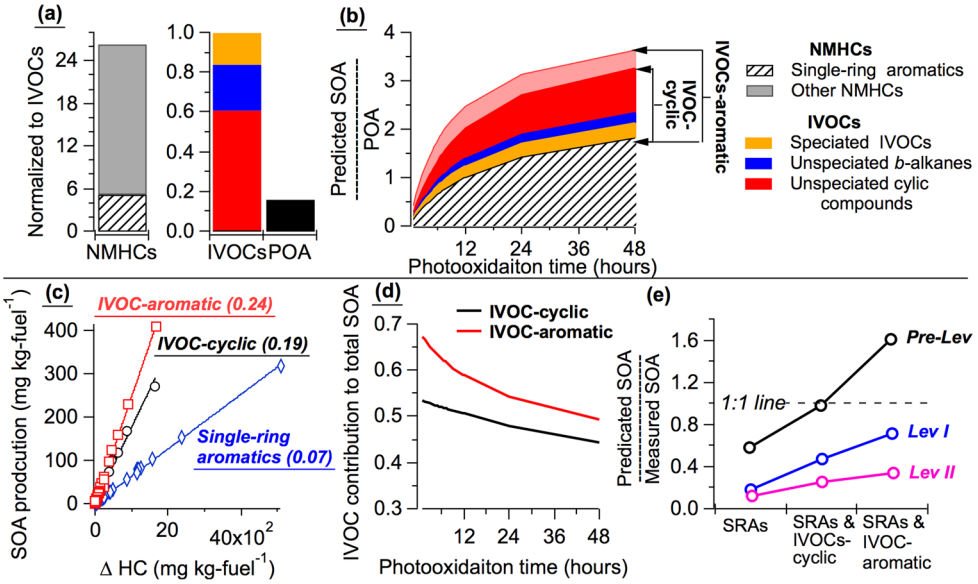

Figure 5. Primary emissions data and predicted SOA production from tailpipe emissions from LDGVs over the cold-start UC: (a) average primary emissions normalized by IVOCs; (b) average predicted SOA-to-POA ratio as a function of photo-oxidation time; (c) scatter plots of predicted SOA production versus the mass of precursor reacted (ΔHC) after 48 h photo-oxidation (see SI Figure S7). The slope of the lines in (c) indicates the effective SOA yield for different classes of precursor. (d) Mass fraction of predicted SOA due to IVOCs as a function of photo-oxidation time; (e) ratio of predicted to measured SOA during chamber experiments with dilute exhaust from LDGVs over the cold-start UC. The OH concentration used in panels (b) to (d) is [OH] = 1.5×10^6 molecules cm^{-3}.

A comparison of the filter and downstream adsorbent samples reveals that the quartz filters only collected only 37 ± 26% of the total (filter + adsorbent) SVOC emissions (Figure 4). This is likely due to a large faction of SVOCs existing as vapors at 47 °C, the sampling temperature used here and specified by emission certification protocols (e.g., CFR 86). Organic vapors are only partially collected by quartz filters. Particulate matter evaporating from the filter (negative sampling artifacts) may also contribute to the low collection efficiency of SVOCs by the quartz filters. Substantial breakthrough of SVOCs from quartz filters was also observed during measurements of emissions from diesel vehicles without a diesel particulate filter.[9] Some of the SVOC vapors not collected by the quartz filters at 47 °C likely condense to form POA in the atmosphere.

We also evaluated the recovery of LVOCs by the GC/MS analysis by comparing the total organic mass quantified by GC/MS analysis to results from EC/OC analysis of the same quartz filter. A strong correlation is found between these two data sets with an R^2 = 0.9 and slope = 0.7. The median of the ratios between the GC/MS and EC/OC analysis for OA is 0.8. This means that, on average, 20−30% of the organics collected on a quartz filter during a LDGV test were unrecovered by the GC/MS analysis. These unrecovered organics are presumably LVOCs that did not desorb at 300 °C during the GC/MS analysis (versus 580 °C during the EC/OC analysis). This amount of unrecovered LVOCs is consistent with thermodenuder measurements.[22] It is also similar to the recovery measured during analysis of samples collected in a traffic tunnel (60% ± 20%)[32] and for emissions in diesel vehicles (57% ± 29%).[9] In comparison to the total amount of low volatility organics collected using quartz filters and Tenax sorbents, the unrecovered LVOCs by the GC/MS analysis are small (only 2.6% of the organics in the volatility range from 3×10^{-2} to 3×10^6 $\mu g/m^3$). However, they can contribute significantly to POA at the ambient conditions. We propose to include the unrecovered LVOCs in the 10^{-2} $\mu g/m^3$ volatility bin which remains in the particle phase at atmospheric conditions (SI Table S5b).

Our results highlight the challenges associated with sampling low-volatility organics. In particular, sampling artifacts make it challenging to define POA emissions using quartz filter samples. The sampling strategy used here, quartz filter followed by sorbent tubes, quantitatively collects all low-volatility organics regardless of phase. Partitioning theory can then be used to estimate the fraction of these organics in the gas and particle phases. In addition, both EC/OC and GC/MS analysis are required to quantify and characterize the organics collected on the quartz filter samples.

SOA Production from IVOCs. In this section we estimate the SOA production from IVOCs and compare it to similar estimates for single-ring aromatics (SRAs) and results from photo-oxidation experiments conducted as part of these experiments.[7] These comparisons examine the importance of IVOCs as SOA precursors and provide insights into the causes for discrepancies between predicted and measured SOA production.

The SOA mass (ΔM, mg/kg-fuel) formed over a period (Δt) is estimated:[9,11]

$$\Delta M = [\mathrm{HC}] \times (1 - e^{-k_{OH} \times [\mathrm{OH}] \times \Delta t}) \times Y$$

where [HC] is the emission factor (mg/kg-fuel) of a SOA precursor; k_{OH} is the precursor OH reaction rate constant at 25 °C; [OH] is the OH concentration (molecules cm^{-3}); and Y is the SOA mass yield under high-NO_x conditions. The total SOA formation is determined by summing the SOA mass formed from all precursors. SOA yields (Y) are based on published smog chamber data[11−14,33] and extrapolated to an OA concentration of 9 $\mu g/m^3$, the average concentration at the end of photo-oxidation experiments. The SOA yields and OH reaction rates of speciated IVOCs and SRAs are listed in SI Tables S6 and S7.

DOI: 10.1021/acs.est.5b06247
Environ. Sci. Technol. 2016, 50, 4554−4563

For this analysis we only include speciated C_6-C_9 SRAs in the SOA model. These SRAs are the ones commonly included in models; they are also measured in the atmosphere.[10] Some larger SRAs ($>C_9$) were also measured during these tests,[19] but they contributed less than 10%, on average, of the C_6-C_9 SRA emissions. Since some of these larger ($>C_9$) aromatic compounds could elute in the B_{12} retention-time-based bin, we did not include them in the SOA model to ensure there was no double counting. This is a conservative assumption, which means we may underestimate the total SOA formation. Research is needed to better understand the relationship between NMHC (collected using a Teflon bag) and IVOC (collected using an adsorbent) measurements.

The SOA yields and OH reaction rate constants of IVOC UCM are estimated following the approach of Zhao et al.[9,10] This approach assigns surrogates to the unspeciated *b*-alkanes and unspeciated cyclic compounds in each of the 11 retention time bins (SI Table S8).[9,10] Surrogates are selected to account for the effects of molecular structure and volatility on SOA yields[12−14] and OH reactivity.[34] For example, the SOA yield and OH reaction rate constant of unspeciated *b*-alkanes in the B_n IVOC bin are represented by the C_{n-2} *n*-alkane and C_n *n*-alkane, respectively.[9,10]

Both aromatic compounds and cyclic alkanes are likely major contributors to unspeciated cyclic compounds in the $B_{12}-B_{16}$ bins (SI Figure S6). Therefore, calculations are performed using two different types of surrogates (*n*-alkanes and naphthalenes) for the unspeciated cyclic compounds in these bins to bound the potential SOA production. For the cyclic-alkane case, the C_n *n*-alkane is used as the surrogate for the unspeciated cyclic compounds in the B_n bin (SI Table S8a). For the aromatic case, naphthalene or methylnaphthalenes are used as the surrogates for the unspeciated cyclic emissions in the B_{12}-B_{16} bins (SI Table S8b). For the higher bins (B_{15} and B_{16}), *n*-alkanes are used to represent SOA yields in the bins for both cases because there is no data in the literature for SOA yields for C_3- and C_4-naphthalenes. For both cases, *n*-alkanes are used to represent the SOA yields and OH reaction rates of unspeciated cyclic compounds in $B_{17}-B_{22}$ bins because the mass spectrum suggests the IVOCs in those bins are dominated by cyclic alkanes (SI Figure S6; Table S8).[9,10] In the following discussion, the label "IVOC-cyclic" indicates IVOCs with the cyclic alkane rich case and the label "IVOC-aromatic" indicates IVOCs with the aromatic rich case.

LDGVs over the Cold-Start UC. Figure 5 summarizes the results from the SOA modeling using LDGV cold-start UC emissions data. Figure 5a presents the primary emissions data from the average LDGV cold-start test that are used as inputs to the model. These data have been normalized to the IVOC EF. The average C_6-C_9 SRA EF is about 5 times higher than IVOC EF and the average POA EF is about 15% that of IVOCs. Given the strong correlations between IVOCs and other pollutants (Figure 3), these average ratios are representative of the relative abundance of different SOA precursors across the entire set of cold-start LDGV tests.

Figure 5b shows the predicted SOA formation as a function of time (assuming an average OH concentration of 1.5×10^6 molecules cm^{-3}).[35] The predicted SOA production exceeds POA emissions after about 4 h photo-oxidation, and is 3.6 times greater than the POA emissions after 48 h photo-oxidation. Therefore, the model predicts that SOA production will dominate over POA emissions as a source of ambient organic aerosol, consistent with results from photo-oxidation experiments with dilute exhaust.[7]

The SOA-to-POA ratio in Figure 5b likely underestimates the actual ratio because SOA yields used here only account for the SOA formation from quasi-first generation oxidation products (i.e., no multigenerational aging) and do not correct for the organic vapor wall losses.[36,37] In addition, the SOA-to-POA ratio is based on POA emissions measured using bare quartz filters collected from the CVS, which are biased high relative to more dilute atmospheric conditions.[22] Correcting for sampling artifacts and partitioning biases would further increase the SOA-to-POA ratio.

The largest contributor to SOA production from IVOCs is unspeciated cyclic compounds followed by speciated IVOCs and unspeciated *b*-alkanes (Figure 5b). Although the total IVOC emissions are substantially less than C_6-C_9 SRAs, the predicted SOA production from IVOCs is comparable to that of C_6-C_9 SRAs due to the much higher SOA yields of IVOCs than C_6-C_9 SRAs (Figure 5b, c).

Figure 5c plots the predicted SOA production versus reacted precursor mass after 48 h of photo-oxidation. The SOA production varies widely from vehicle to vehicle because of differences in the magnitude in precursor emissions, not because of differences in precursor composition. This is demonstrated by the strong correlation of SOA production ($R^2 > 0.99$) to the reacted IVOC mass across the entire set of vehicles.

The ratio of SOA production to the mass of SOA precursors reacted is the effective SOA yield. The slopes plotted in Figure 5c are the effective SOA yields for different classes of precursors after 48 h photo-oxidation. The average effective SOA yield from IVOCs is 0.19 ± 0.03 for IVOC-cyclic and 0.24 ± 0.03 for IVOC-aromatic, both of which are substantially greater than the yield for C_6-C_9 SRAs (0.07 ± 0.002). The effective SOA yield of IVOCs varies modestly with increasing oxidation (time) due to differences in OH reaction rates and SOA yields for speciated and unspeciated IVOCs. This variation does not affect the overall finding that IVOCs make a substantial contribution to SOA.

Figure 5d shows that the relative contribution of IVOCs to total SOA production is initially much higher than that of C_6-C_9 SRAs but then decreases with increasing OH exposure. IVOCs react faster than C_6-C_9 SRAs and most of IVOCs have been oxidized within 12 h of photo-oxidation (68% IVOC-cyclic and 80% IVOC-aromatic versus 48% SRAs). After 48 h of photo-oxidation, just about half of the SOA production is predicted to come from IVOCs (43% ± 19% for IVOC-cyclic and 49% ± 18% for IVOC-aromatic). The substantial contributions of IVOCs to total SOA production clearly demonstrate the importance of including IVOCs in SOA models.

Hot-Start Cycles and SOREs. Model calculations were also performed using hot-start and SORE emissions data. The differences in predicted SOA production between the different tests (e.g., hot versus cold start) were driven by differences in the emission rate not precursor composition. The modest effect of IVOC composition is reflected by the similarity in effective SOA yields across the set of tests (SI Figure S7); for example, the effective SOA yield for IVOC-aromatic after 48 h of photo-oxidation is 0.24 ± 0.03 for the cold-start UC emissions, 0.27 ± 0.02 for the hot start emissions, and 0.25 ± 0.01 for the SORE tests.

DOI: 10.1021/acs.est.5b06247
Environ. Sci. Technol. 2016, 50, 4554−4563

The relative importance of IVOCs versus C_6-C_9 SRAs as SOA precursors depends on the ratio of total-IVOC emissions to total NMHC emissions. The higher IVOC-to-NMHC ratio of emissions for hot- versus cold-start UC means that the IVOCs are an even more important class of SOA precursors for hot-start operations. For example, after 3 h photo-oxidation, the SOA production from IVOCs is predicted to be 4 times greater than C_6-C_9 SRAs for the hot-start cycles versus only ~2 for the cold-start UC.

Comparison between Predicted and Measured SOA. Figure 5e compares model predictions to measured SOA production during chamber experiments conducted at the same time as the IVOC sampling. These chamber experiments were conducted with dilute exhaust from LDGVs over the cold-start UC under high-NO_x conditions.[7] The comparisons are for averages for the three different classes of LDGVs (comparisons for individual experiments are presented in SI Figure S8). Model predictions are shown for three different combinations of SOA precursors: SRAs; SRAs + IVOC-cyclic; and SRAs + IVOC-aromatic.

Traditionally C_6-C_9 SRAs have been thought to be the dominant class of SOA precursors in LDGV exhaust.[4,6] If SRAs are the only class of SOA precursors, then the model underpredicts the measured SOA production by 40−90%, with larger discrepancies for newer (LEV2) vehicles (Figure 5e). Including IVOCs in the model substantially increases the predicted SOA mass. However, about 30% and 65% of SOA measured during chamber experiments with LEV1 and LEV2 vehicles remains unexplained. Adding IVOCs to the model causes it to overpredict the SOA production from Pre-LEV vehicles. The fact that the model overpredicts SOA formation for the Pre-LEV vehicles versus underpredicting it for newer vehicles (LEV1 and LEV2) means that there are competing factors whose relative importance systematically varies across the set of experiments.

Several factors could cause the model to underestimate SOA production. First, the approach of Zhao et al.[9,10] may provide a conservative estimate of SOA production from IVOCs. For example, it likely overestimates the contribution of unspeciated *b*-alkanes to the emissions; *b*-alkanes have lower SOA yields than cyclic compounds in the same retention-time bin.[9,10] Second, there may be additional SOA precursors not included in the model such as SVOCs. SVOC EFs correspond to 27% ± 16% and 41% ± 25% of IVOC EFs for LEV1 and LEV2 vehicles, respectively. Another class of precursors not included in the model could be other unspeciated organic vapors in addition to IVOCs and SVOCs. About 25% of NMHC emissions were not resolved into a molecular lever.[19] The IVOCs and SVOCs measured here only correspond to about one-quarter of these unspeciated NMHC emissions. Finally, the chamber conditions could also cause the discrepancies. For example, SOA yields of IVOCs and SRAs in dilute exhaust, a complex mixture of NO_x and organics, could be substantially higher than those derived from chamber experiments with individual compounds used in the model.

Losses of IVOCs in the transfer line to the smog chamber could cause the model to overpredict SOA production. Dilute exhaust was drawn from the CVS and injected into the smog chamber through a electrically heated silcosteel transfer line (~47 °C, matching the temperature of the CVS).[7] In contrast, the IVOC emissions used as inputs to the model were measured directly from the CVS, upstream of the smog chamber transfer line. Wall losses of IVOC have been reported by previous studies.[9,38] Losses in the transfer line would reduce the IVOC concentrations inside the smog chamber relative to CVS, especially IVOCs with lower volatility.[38−40] This SOA model also overpredicted the SOA formation from dilute diesel vehicle exhaust measured using the same experimental setup.[9]

Gasoline versus Diesel IVOCs. Zhao et al.[9] characterized diesel IVOC emissions using the same techniques as this study. A comparison with the LDGV data reveals important differences between gasoline and diesel IVOC emissions. First, IVOCs contribute a much larger fraction of the NMHC emissions from diesel vehicles (60%) than LDGVs (4% for cold-start UC to 17% for hot-start tests). Therefore, for diesel emissions, IVOCs are the dominant class of SOA precursors creating more than 95% of the estimated SOA mass versus about 50% for LDGVs (Figure 5b).

There are also differences in the IVOC composition and volatility distribution of gasoline and diesel exhaust. The IVOC emissions in diesel are dominated by aliphatic compounds while gasoline exhaust has a more substantial aromatic component.[9] Diesel exhaust also has a much broader IVOC volatility distribution than LDGV exhaust, with much higher emissions in the $B_{13}-B_{18}$ bins.[9] In comparison to diesel, IVOCs in LDGV exhaust are skewed much more toward higher volatility compounds (B_{12} bin). These differences reflect the underlying differences in the two fuels.

Implications. Our results demonstrate that IVOCs are an important class of organic emissions from LDGVs and SOREs, adding to the growing body of research on the importance of IVOC emissions from combustion sources.[2,9] Although IVOCs only correspond to a small fraction of the total NMHC emissions, they contribute as much or more SOA than traditional precursors such as SRAs because of their high SOA yields. Therefore, inclusion of IVOCs into SOA models should substantially improve the agreement between predicted and measured SOA in the atmosphere. The consistency in the IVOC volatility distribution and chemical composition across the set of tests and the well-constrained ratios of IVOCs to other pollutants not only simplifies the parametrization of IVOCs for use in SOA models, but also can be used to develop IVOC emission inventories.

■ ASSOCIATED CONTENT

Supporting Information

The Supporting Information is available free of charge on the ACS Publications website at DOI: 10.1021/acs.est.5b06247.

Tables for emission factors of IVOCs in each test, OH reaction rate constants and SOA yields used in estimation of SOA production and other data used in this study (DOCX)
(XLSX)

■ AUTHOR INFORMATION

Corresponding Author

*E-mail: alr@andrew.cmu.edu.

Present Addresses

[§](C.J.H.) Department of Chemical, Biochemical and Environmental Engineering at the University of Maryland, Baltimore County, Maryland, 21250, United States.

[∥](A.A.M.) Department of Civil, Environmental, and Geodetic Engineering, The Ohio State University, Columbus, Ohio, United States

DOI: 10.1021/acs.est.5b06247
Environ. Sci. Technol. 2016, 50, 4554−4563

Notes

The authors declare no competing financial interest.

■ ACKNOWLEDGMENTS

We thank the excellent and dedicated personnel at the California Air Resources Board, especially at the Haagen-Smit Laboratory. The California Air Resources Board provided substantial in-kind support for vehicle procurement, testing and emissions characterization. Carnegie Mellon University was supported by the US Environmental Protection Agency National Center for Environmental Research through the STAR program (Project RD834554). The views, opinions, and/or findings contained in this paper are those of the authors and should not be construed as an official position of the funding agencies.

■ REFERENCES

(1) Bahreini, R.; Middlebrook, A. M.; de Gouw, J. A.; Warneke, C.; Trainer, M.; Brock, C. A.; Stark, H.; Brown, S. S.; Dube, W. P.; Gilman, J. B.; Hall, K.; Holloway, J. S.; Kuster, W. C.; Perring, A. E.; Prevot, A. S. H.; Schwarz, J. P.; Spackman, J. R.; Szidat, S.; Wagner, N. L.; Weber, R. J.; Zotter, P.; Parrish, D. D. Gasoline emissions dominate over diesel in formation of secondary organic aerosol mass. *Geophys. Res. Lett.* **2012**, *39*, L06805.

(2) Jathar, S. H.; Gordon, T. D.; Hennigan, C. J.; Pye, H. O. T.; Pouliot, G.; Adams, P. J.; Donahue, N. M.; Robinson, A. L. Unspeciated organic emissions from combustion sources and their influence on the secondary organic aerosol budget in the United States. *Proc. Natl. Acad. Sci. U. S. A.* **2014**, *111* (29), 10473−10478.

(3) McDonald, B. C.; Goldstein, A. H.; Harley, R. A. Long-Term Trends in California Mobile Source Emissions and Ambient Concentrations of Black Carbon and Organic Aerosol. *Environ. Sci. Technol.* **2015**, *49* (8), 5178−5188.

(4) Gentner, D. R.; Isaacman, G.; Worton, D. R.; Chan, A. W. H.; Dallmann, T. R.; Davis, L.; Liu, S.; Day, D. A.; Russell, L. M.; Wilson, K. R.; Weber, R.; Guha, A.; Harley, R. A.; Goldstein, A. H. Elucidating secondary organic aerosol from diesel and gasoline vehicles through detailed characterization of organic carbon emissions. *Proc. Natl. Acad. Sci. U. S. A.* **2012**, *109* (45), 18318−18323.

(5) Kroll, J. H.; Seinfeld, J. H. Chemistry of secondary organic aerosol: Formation and evolution of low-volatility organics in the atmosphere. *Atmos. Environ.* **2008**, *42* (16), 3593−3624.

(6) Odum, J. R.; Jungkamp, T. P. W.; Griffin, R. J.; Flagan, R. C.; Seinfeld, J. H. The atmospheric aerosol-forming potential of whole gasoline vapor. *Science* **1997**, *276* (5309), 96−99.

(7) Gordon, T. D.; Presto, A. A.; May, A. A.; Nguyen, N. T.; Lipsky, E. M.; Donahue, N. M.; Gutierrez, A.; Zhang, M.; Maddox, C.; Rieger, P.; Chattopadhyay, S.; Maldonado, H.; Maricq, M. M.; Robinson, A. L. Secondary organic aerosol formation exceeds primary particulate matter emissions for light-duty gasoline vehicles. *Atmos. Chem. Phys.* **2014**, *14* (9), 4661−4678.

(8) Platt, S. M.; El Haddad, I.; Zardini, A. A.; Clairotte, M.; Astorga, C.; Wolf, R.; Slowik, J. G.; Temime-Roussel, B.; Marchand, N.; Jezek, I.; Drinovec, L.; Mocnik, G.; Mohler, O.; Richter, R.; Barmet, P.; Bianchi, F.; Baltensperger, U.; Prevot, A. S. H. Secondary organic aerosol formation from gasoline vehicle emissions in a new mobile environmental reaction chamber. *Atmos. Chem. Phys.* **2013**, *13* (18), 9141−9158.

(9) Zhao, Y.; Nguyen, N. T.; Presto, A. A.; Hennigan, C. J.; May, A. A.; Robinson, A. L. Intermediate volatility organic compound emissions from on-road diesel vehicles: chemical composition, emission factors, and estimated secondary organic aerosol production. *Environ. Sci. Technol.* **2015**, *49* (19), 11516−11526.

(10) Zhao, Y. L.; Hennigan, C. J.; May, A. A.; Tkacik, D. S.; de Gouw, J. A.; Gilman, J. B.; Kuster, W. C.; Borbon, A.; Robinson, A. L. Intermediate-Volatility Organic Compounds: A Large Source of Secondary Organic Aerosol. *Environ. Sci. Technol.* **2014**, *48* (23), 13743−13750.

(11) Chan, A. W. H.; Kautzman, K. E.; Chhabra, P. S.; Surratt, J. D.; Chan, M. N.; Crounse, J. D.; Kurten, A.; Wennberg, P. O.; Flagan, R. C.; Seinfeld, J. H. Secondary organic aerosol formation from photooxidation of naphthalene and alkylnaphthalenes: implications for oxidation of intermediate volatility organic compounds (IVOCs). *Atmos. Chem. Phys.* **2009**, *9* (9), 3049−3060.

(12) Hunter, J. F.; Carrasquillo, A. J.; Daumit, K. E.; Kroll, J. H. Secondary Organic Aerosol Formation from Acyclic, Monocyclic, and Polycyclic Alkanes. *Environ. Sci. Technol.* **2014**, *48*, 10227−10234.

(13) Lim, Y. B.; Ziemann, P. J. Effects of Molecular Structure on Aerosol Yields from OH Radical-Initiated Reactions of Linear, Branched, and Cyclic Alkanes in the Presence of NOx. *Environ. Sci. Technol.* **2009**, *43* (7), 2328−2334.

(14) Presto, A. A.; Miracolo, M. A.; Donahue, N. M.; Robinson, A. L. Secondary Organic Aerosol Formation from High-NOx Photo-Oxidation of Low Volatility Precursors: n-Alkanes. *Environ. Sci. Technol.* **2010**, *44* (6), 2029−2034.

(15) Tkacik, D. S.; Lambe, A. T.; Jathar, S.; Li, X.; Presto, A. A.; Zhao, Y. L.; Blake, D.; Meinardi, S.; Jayne, J. T.; Croteau, P. L.; Robinson, A. L. Secondary Organic Aerosol Formation from in-Use Motor Vehicle Emissions Using a Potential Aerosol Mass Reactor. *Environ. Sci. Technol.* **2014**, *48* (19), 11235−11242.

(16) Stroud, C. A.; Liggio, J.; Zhang, J.; Gordon, M.; Staebler, R. M.; Makar, P. A.; Zhang, J. H.; Li, S. M.; Mihele, C.; Lu, G.; Wang, D. K.; Wentzell, J.; Brook, J. R.; Evans, G. J. Rapid organic aerosol formation downwind of a highway: Measured and model results from the FEVER study. *J. Geophys. Res.* **2014**, *119* (3), 1663−1679.

(17) Schauer, J. J.; Kleeman, M. J.; Cass, G. R.; Simoneit, B. R. T. Measurement of emissions from air pollution sources. 5. C-1-C-32 organic compounds from gasoline-powered motor vehicles. *Environ. Sci. Technol.* **2002**, *36* (6), 1169−1180.

(18) Ban-Weiss, G. A.; McLaughlin, J. P.; Harley, R. A.; Lunden, M. M.; Kirchstetter, T. W.; Kean, A. J.; Strawa, A. W.; Stevenson, E. D.; Kendall, G. R. Long-term changes in emissions of nitrogen oxides and particulate matter from on-road gasoline and diesel vehicles. *Atmos. Environ.* **2008**, *42* (2), 220−232.

(19) May, A. A.; Nguyen, N. T.; Presto, A. A.; Gordon, T. D.; Lipsky, E. M.; Karve, M.; Gutierrez, A.; Robertson, W. H.; Zhang, M.; Brandow, C.; Chang, O.; Chen, S. Y.; Cicero-Fernandez, P.; Dinkins, L.; Fuentes, M.; Huang, S. M.; Ling, R.; Long, J.; Maddox, C.; Massetti, J.; McCauley, E.; Miguel, A.; Na, K.; Ong, R.; Pang, Y. B.; Rieger, P.; Sax, T.; Truong, T.; Vo, T.; Chattopadhyay, S.; Maldonado, H.; Maricq, M. M.; Robinson, A. L. Gas- and particle-phase primary emissions from in-use, on-road gasoline and diesel vehicles. *Atmos. Environ.* **2014**, *88*, 247−260.

(20) Hodzic, A.; Jimenez, J. L.; Madronich, S.; Canagaratna, M. R.; DeCarlo, P. F.; Kleinman, L.; Fast, J. Modeling organic aerosols in a megacity: potential contribution of semi-volatile and intermediate volatility primary organic compounds to secondary organic aerosol formation. *Atmos. Chem. Phys.* **2010**, *10* (12), 5491−5514.

(21) Pye, H. O. T.; Seinfeld, J. H. A global perspective on aerosol from low-volatility organic compounds. *Atmos. Chem. Phys.* **2010**, *10* (9), 4377−4401.

(22) May, A. A.; Presto, A. A.; Hennigan, C. J.; Nguyen, N. T.; Gordon, T. D.; Robinson, A. L. Gas-particle partitioning of primary organic aerosol emissions: (1) Gasoline vehicle exhaust. *Atmos. Environ.* **2013**, *77*, 128−139.

(23) Gordon, T. D.; Tkacik, D. S.; Presto, A. A.; Zhang, M.; Jathar, S. H.; Nguyen, N. T.; Massetti, J.; Truong, T.; Cicero-Fernandez, P.; Maddox, C.; Rieger, P.; Chattopadhyay, S.; Maldonado, H.; Maricq, M. M.; Robinson, A. L. Primary Gas- and Particle-Phase Emissions and Secondary Organic Aerosol Production from Gasoline and Diesel Off-Road Engines. *Environ. Sci. Technol.* **2013**, *47* (24), 14137−14146.

(24) May, A. A.; Presto, A. A.; Hennigan, C. J.; Nguyen, N. T.; Gordon, T. D.; Robinson, A. L. Gas-Particle Partitioning of Primary Organic Aerosol Emissions: (2) Diesel Vehicles. *Environ. Sci. Technol.* **2013**, *47* (15), 8288−8296.

DOI: 10.1021/acs.est.5b06247
Environ. Sci. Technol. 2016, 50, 4554−4563

(25) Aiken, A. C.; Decarlo, P. F.; Kroll, J. H.; Worsnop, D. R.; Huffman, J. A.; Docherty, K. S.; Ulbrich, I. M.; Mohr, C.; Kimmel, J. R.; Sueper, D.; Sun, Y.; Zhang, Q.; Trimborn, A.; Northway, M.; Ziemann, P. J.; Canagaratna, M. R.; Onasch, T. B.; Alfarra, M. R.; Prevot, A. S. H.; Dommen, J.; Duplissy, J.; Metzger, A.; Baltensperger, U.; Jimenez, J. L. O/C and OM/OC ratios of primary, secondary, and ambient organic aerosols with high-resolution time-of-flight aerosol mass spectrometry. *Environ. Sci. Technol.* **2008**, *42* (12), 4478−4485.
(26) Davis, S. C.; Diegel, S. W.; Boundy, R. G. Transportation energy data book (Oak Ridge National Laboratory, Oak Ridge, Tennessee). http://cta.ornl.gov/data/index.shtml (accessed January 2014).
(27) NIST, http://webbook.nist.gov/chemistry/name-ser.html.
(28) Prestch, E.; Buhlmann, P.; Badertscher, M. *Structure Determination of Organic Compounds: Tables of Spectral Data*, 4th ed.; Springer; 2009.
(29) Robinson, A. L.; Donahue, N. M.; Shrivastava, M. K.; Weitkamp, E. A.; Sage, A. M.; Grieshop, A. P.; Lane, T. E.; Pierce, J. R.; Pandis, S. N. Rethinking organic aerosols: Semivolatile emissions and photochemical aging. *Science* **2007**, *315* (5816), 1259−1262.
(30) Donahue, N. M.; Robinson, A. L.; Pandis, S. N. Atmospheric organic particulate matter: From smoke to secondary organic aerosol. *Atmos. Environ.* **2009**, *43* (1), 94−106.
(31) Turpin, B. J.; Saxena, P.; Andrews, E. Measuring and simulating particulate organics in the atmosphere: problems and prospects. *Atmos. Environ.* **2000**, *34* (18), 2983−3013.
(32) Worton, D. R.; Isaacman, G.; Gentner, D. R.; Dallmann, T. R.; Chan, A. W. H.; Ruehl, C.; Kirchstetter, T. W.; Wilson, K. R.; Harley, R. A.; Goldstein, A. H. Lubricating Oil Dominates Primary Organic Aerosol Emissions from Motor Vehicles. *Environ. Sci. Technol.* **2014**, *48* (7), 3698−3706.
(33) Ng, N. L.; Kroll, J. H.; Chan, A. W. H.; Chhabra, P. S.; Flagan, R. C.; Seinfeld, J. H. Secondary organic aerosol formation from m-xylene, toluene, and benzene. *Atmos. Chem. Phys.* **2007**, *7* (14), 3909−3922.
(34) Kwok, E. S. C.; Atkinson, R. Estimation of Hydroxyl Radical Reaction-Rate Constants for Gas-Phase Organic-Compounds Using a Structure-Reactivity Relationship - an Update. *Atmos. Environ.* **1995**, *29* (14), 1685−1695.
(35) Hayes, P. L.; Ortega, A. M.; Cubison, M. J.; Froyd, K. D.; Zhao, Y.; Cliff, S. S.; Hu, W. W.; Toohey, D. W.; Flynn, J. H.; Lefer, B. L.; Grossberg, N.; Alvarez, S.; Rappenglueck, B.; Taylor, J. W.; Allan, J. D.; Holloway, J. S.; Gilman, J. B.; Kuster, W. C.; De Gouw, J. A.; Massoli, P.; Zhang, X.; Liu, J.; Weber, R. J.; Corrigan, A. L.; Russell, L. M.; Isaacman, G.; Worton, D. R.; Kreisberg, N. M.; Goldstein, A. H.; Thalman, R.; Waxman, E. M.; Volkamer, R.; Lin, Y. H.; Surratt, J. D.; Kleindienst, T. E.; Offenberg, J. H.; Dusanter, S.; Griffith, S.; Stevens, P. S.; Brioude, J.; Angevine, W. M.; Jimenez, J. L. Organic aerosol composition and sources in Pasadena, California, during the 2010 CalNex campaign. *J. Geophys. Res.* **2013**, *118* (16), 9233−9257.
(36) Aumont, B.; Camredon, M.; Mouchel-Vallon, C.; La, S.; Ouzebidour, F.; Valorso, R.; Lee-Taylor, J.; Madronich, S. Modeling the influence of alkane molecular structure on secondary organic aerosol formation. *Faraday Discuss.* **2013**, *165*, 105−122.
(37) Zhang, X.; Cappa, C. D.; Jathar, S. H.; Mcvay, R. C.; Ensberg, J. J.; Kleeman, M. J.; Seinfeld, J. H. Influence of vapor wall loss in laboratory chambers on yields of secondary organic aerosol. *Proc. Natl. Acad. Sci. U. S. A.* **2014**, *111* (16), 5802−5807.
(38) Helmig, D.; Revermann, T.; Pollmann, J.; Kaltschmidt, O.; Hernandez, A. J.; Bocquet, F.; David, D. Calibration system and analytical considerations for quantitative sesquiterpene measurements in air. *Journal of Chromatography A* **2003**, *1002* (1−2), 193−211.
(39) Goss, K. U.; Schwarzenbach, R. P. Gas/solid and gas/liquid partitioning of organic compounds: Critical evaluation of the interpretation of equilibrium constants. *Environ. Sci. Technol.* **1998**, *32* (14), 2025−2032.
(40) Matsunaga, A.; Ziemann, P. J. Gas-Wall Partitioning of Organic Compounds in a Teflon Film Chamber and Potential Effects on Reaction Product and Aerosol Yield Measurements. *Aerosol Sci. Technol.* **2010**, *44* (10), 881−892.

DOI: 10.1021/acs.est.5b06247
Environ. Sci. Technol. 2016, 50, 4554−4563